ELSEVIER

Contents lists available at ScienceDirect

# International Communications in Heat and Mass Transfer

MEAN MASS TRANSFER

journal homepage: www.elsevier.com/locate/ichmt

# Confinement size dependency of flow structures and thermal characteristics in turbulent impinging air jet on a flat target surface

Vijaykumar Nagathan <sup>a</sup>, Mohammed Khalifa <sup>a,b,\*</sup>, Basavaraj M. Angadi <sup>a</sup>, Meda Adimurthy <sup>a</sup>, Vadiraj Katti <sup>a</sup>

#### ARTICLE INFO

#### Keywords: Impinging jet Confinement Sub-atmospheric Heat transfer Turbulent flow

#### ABSTRACT

Impinging jets are of significant interest because of their facile design and high heat transfer rates and enabling effective cooling. Impinging jets are specifically designed to be suitable for various industrial processes that require high heat transfer rates. In this study, an experimental study was carried out to evaluate the impact of confinement size on the wall static pressure coefficient (Cp) distribution and Nusselt number (Nu) of a turbulent air jet impinging on a flat surface. Various confinement sizes ( $C_L/d = 0.0$  to 15.0) and nozzle to target distance (z/d) ratios (0.5 to 6.0) were tested. For both unconfined and confined jets, Cp was highest at stagnation and decreased as the jet flows laterally. Sub-atmospheric pressure zones were observed for confined jet and became stronger with increasing C<sub>L</sub>/d ratio. Nu values at stagnation decreased with increasing confinements, while a secondary peak in Nu was influenced by confinement size and z/d spacing. The secondary peak intensified with confinement up to  $C_L/d = 12.0$ , thereafter it weakened, and shifted towards the stagnation point with larger confinements. At z/d = 6.0, heat transfer at stagnation increased with confinement. Overall, the maximum increase in Nu value was 5.68 % with a thermal performance factor of 1.42 achieved upon confinement ( $C_{\rm I}/d$ 9.0) compared to unconfined jet. Moreover, the results indicate that maintaining the confinement size smaller than the target surface is vital for achieving better heat transfer performance. This study provides critical insights for optimizing impinging jet systems, revealing the nuanced interplay between fluid dynamics and heat transfer coefficients.

# 1. Introduction

Increasing the heat transfer efficiency of various cooling devices is of significant interest in various industries and engineering applications. Among various techniques, impinging air jets have been the subject of significant interest due to their extensive engineering purpose as an effective promoter of heat and mass transport. Impinging jets are implemented in various engineering applications including surface cooling of tubes, pipes, billets, gas turbine blades, food processing industries and aircraft cooling systems. Jet impingement with the air/liquid is imparted onto the surface that requires cooling. The jet exiting with a desirable temperature and velocity impinged directly onto the heated surface having known parameters [1–3]. Jet coming out of a nozzle can be of single or multiple nozzles with different geometries and

sizes. The air jet impingement technique is commonly employed for targeted cooling of surfaces that emit significant heat flux. The air jet flow can be divided into four primary zones. The first zone is the free flow region, characterized by a uniform velocity distribution. The second region is the decaying region, where the jet begins to spread. The third zone is the stagnation zone, occurring where the jet impinges. The fourth and final region is the near-wall flow [4,5]. Nozzles with circular, elliptical, rectangular and squared cross sections are most commonly applied. There are various parameters involved in achieving desirable heat transfer efficiency including surface temperature, jet velocity, air jet temperature, nozzle geometry, flow behavior, target surface roughness etc. Furthermore, conditions such as inter-plate distance between jet to target plate (z/d), lateral flow dynamics, nozzle diameter, nozzle length, jet velocity etc., influence the heat transfer rates [6,7]. Flow

E-mail address: m.khalifa@wood-kplus.at (M. Khalifa).

https://doi.org/10.1016/j.icheatmasstransfer.2025.109683

a B. L. D. E. A's V.P. Dr. P. G. Halakatti College of Engineering and Technology (Affiliated to Visvesvaraya Technological University, Belagavi), Vijayapur, Karnataka,

<sup>&</sup>lt;sup>b</sup> Kompetenzzentrum Holz GmbH, Altenberger Strasse 69, Linz 4040, Austria

<sup>\*</sup> Corresponding author at: B. L. D. E. A's V.P. Dr. P. G. Halakatti College of Engineering and Technology (Affiliated to Visvesvaraya Technological University, Belagavi), Vijayapur, Karnataka, India.

dynamics and heat transfer efficiency of impinging jet also depends on the jets impinged with confined and unconfined boundary [8,9]. Turbulent, round impinging air jets are extensively utilized in practical cooling and drying applications, and their heat transfer characteristics have been the focus of numerous studies. Early investigations offered significant contributions focused on unconfined impinging air jet with different configurations, geometries and parameters. Lytle and Webb [10] reported that the acceleration of fluid between the z/d ratios significantly enhances local turbulence, resulting in increased local heat transfer. Depending on the Re, primary and secondary maxima in heat transfer coefficients are observed. The secondary maxima shift radially outward with larger nozzle-plate spacings and higher jet Re. An investigation was conducted to determine the heat transfer coefficients of flat smooth target plate with round circular nozzle having a fully developed flow at different Re ( $\langle 12,000 \rangle$ ). The stagnation point Nu values decreased monotonically with the increase in z/d ratio of 4.0, while it increased when the spacing ratio was kept at 6.0 [11]. For a specific z/d ratio, the wall pressure factor (Cp) remains unaffected by the Re. However, the heat transfer coefficient at the stagnation point rises with an increase in Re, regardless of the z/d ratio [12–14]. Moreover, the flow dynamics generated by confined impinging air jets differ from those produced by unconfined impinging jets. This difference arises partly because the confining plate influences the entrainment into the jet, resulting in the formation of a recirculating flow region beneath the confining plate. In another study, it was reported that the confined jet reduces the heat transfer rate due to flow constriction [15]. In the confinement configuration, a z/d ratio of 6.0 provides the reasonable heat transfer performance for a circular jet. Furthermore, compared to non-circular jet, circular jet offer better heat transfer performance [16]. Conversely, at smaller z/d ratios, the crossflow can enhance the heat transfer coefficient. This improvement occurs because the mixing with the crossflow stream increases the jet centerline intensity [17]. In confined jets, at lower jet exit to target plate spacings, sub-atmospheric pressure was observed and became stronger as Re increased, which influence the heat transfer coefficients [18]. Furthermore, a toroidal recirculation zone was observed due to the confinement. The recirculation zone shifted radially outward, with the raise in Re and jet exit to plate spacings. The maximum turbulence was observed at a radial distance (r/d) of 2 [19]. Therefore, it can be concluded that there is a linkage existing between turbulence intensity, pressure distribution and heat transfer in confined jets. Youn et.al [20] demonstrated that the degree of confinement of micro jets with a low *Re* conditions (<5600) significantly alter the heat transfer coefficients. The local heat transfer coefficients were found to be reduced in the case of a confined jet compared to an unconfined microjet. In another study, it was found that the low z/d spacing, the intense recirculation disrupted the development of the wall jet. The radial position of the recirculation core aligned with the point where the wall jet velocity had decreased [21]. Further, the confined jet was found to decrease the *Nu* at the stagnation point [22]. The confinement effect typically reduces the average heat transfer, although an increase in heat transfer is observed at low z/d values.

From the literature perspective, there is no clear agreement on the exact confinement effect on the heat transfer performance of impinging jets. Moreover, previous studies lack comprehensive investigations into the fluid flow characteristics of confined jets and their direct influence on heat transfer performance. While many works have examined the influence of confinement on recirculation patterns and heat transfer distribution in impinging air jets, detailed analyses of the specific effects of confinement are scarce.

Considerable uncertainty remains regarding the overall influence of confinement of jet on heat transfer coefficients and wall static pressure distributions in impinging air jets. Some studies reported positive effects on heat transfer rates, whereas others present contradictory findings. Furthermore, no comprehensive study has examined the correlation between confinement size, *Re*, fluid flow behavior and heat transfer coefficients. In fact, several investigations have used confinement sizes

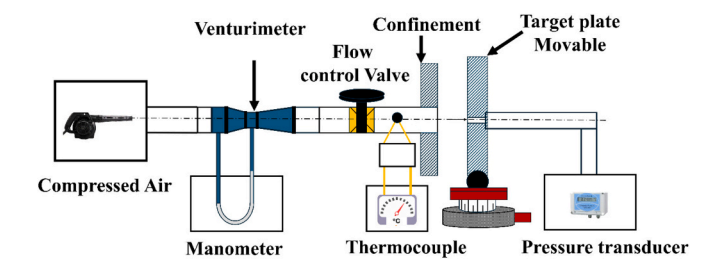


Fig. 1. Schematic diagram of the setup employed for assessing Cp distribution.

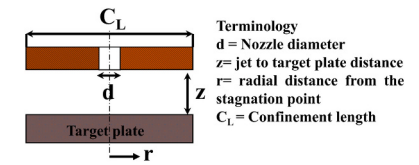


Fig. 2. Schematic depicting confinement and target plate setup with terminologies used in this study.

equal to or larger than the target plate, with most conducted at low Re and often neglecting the critical transition from stagnation to wall-jet regions (r/d > 1.25), where sub-atmospheric pressure zones have been reported. There is no clear understanding on how the confinement size effects the overall performance of impinging jet, especially an optimum configuration is vital in achieving high heat transfer rates. Therefore, we believe it is important to address this critical gap by providing a comprehensive, detailed analysis of both the fluid flow and heat transfer characteristics of turbulent confined impinging jets across a wide range of confinement sizes, z/d spacings, r/d values, and Re numbers.

With the above motivation, this work focuses on the impact of confinement size on wall static pressure and heat transfer distribution in high turbulence impinging air jets on a smooth, flat target surface. A detailed study was conducted to explore the interactions between the Re, z/d ratio, lateral distance from the centerline axis (r), and the degree of confinement ( $C_L/d$ ) on wall static pressure and heat transfer distribution. Based on a comprehensive literature review, the parameters varied were z/d from 0.0 to 6.0, r/d from 0.0 to 4.0, and  $C_L/d$  from 0.0 to 15.0. Additionally, an independence test was performed to confirm the influence of the Re on wall static pressure distribution. This comprehensive approach provides new insights into the role of confinement in impinging jet flows, contributing valuable knowledge to the field and addressing the gaps identified in previous studies.

# 2. Experimental details

## 2.1. Experimental test set-up

The experimental setup for determining fluid flow studies (pressure coefficients, Cp) is illustrated schematically in Fig. 1. In this study, air was discharged through a long aluminum pipe nozzle with a length of 75 cm and a diameter of 1.65 cm ensuring fully developed flow. To control the flow rate, needle valves were connected to Venturi meter and monitored using differential pressure transducer [Furness Controls Limited, Mech-tech Marketing Pvt., India]. The impingement target plate (25 cm  $\times$  25 cm  $\times$  1 cm) was constructed from acrylic sheet.

A fully developed air jet strikes the target plate at a specified distance from the nozzle exit (z) and then disperses into the surrounding room air. The study examines various inter-plate distance (nozzle exit to impingement plate distance) (z/d) ratios: 0.5, 1.0, 2.0, 4.0, and 6.0. Fig. 2 shows the schematic illustration of confinement and target plate setup with the terminologies used in this study. A traversing table was used for the axial and radial movement of the target plate from the

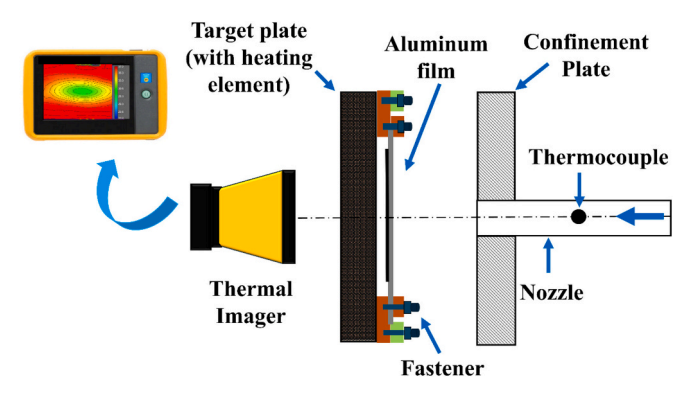


**Fig. 3.** Schematic illustration of the setup used for the evaluation of heat transfer characteristics.

nozzle exit and the corresponding Cp was measured using a Ø 0.5 mm pressure tap located at the center of the impingement plate. The  $C_p$  was calculated using the following equation:

$$C_p = \frac{\Delta_p}{0.5 \times \rho \times V_j^2} \tag{1}$$

Where,  $\Delta p$  is the local pressure exerted on the impinging surface;  $V_j$  is the average jet velocity; and  $\rho$  is the air density.

Fig. 3 illustrates the experimental setup utilized for assessing local heat transfer characteristics. A stainless-steel foil target plate, measuring  $160 \text{ mm} \times 80 \text{ mm} \times 0.06 \text{ mm}$  was securely clamped between two copper bus bars. Given the insignificant thickness of the foil, lateral conduction was assumed to be insignificant, providing a constant heat flux, a condition confirmed by several studies [10]. A high-precision thermal imager [Fluke Ti 55 IR Fusion Technology, USA]  $320 \times 240$  mm focal plane array with 25-µm pitch detector and spatial resolution of 1.30 mrad was positioned opposite the target plate to capture thermal images. Since the foil thickness was negligible, thermal images are taken from the back-side of the impingement surface, which was painted with matte finish black paint (Asian paints, India). The foil was heated by adjusting the power supply with a dimmerstat (voltage-current regulator, Meco Instruments, India), and the air temperature from the jet is monitored using a K-type thermocouple. At least five images were captured to confirm the reproducibility of the results.

The uncertainty analysis for measuring local heat transfer and fluid flow parameters was performed following the methodology reported in the literature [23–25]. The calculated uncertainty values for all measured and derived quantities are provided in the supplementary information (Table S1). The Nusselt number (*Nu*) for the surface was

determined with the following equations.

$$N_u = \frac{hd}{k} \tag{2}$$

$$h = \frac{q_{conv}}{T_r - T_i} \tag{3}$$

Where, h: heat transfer coefficient (W/m $^2$  K); k: thermal conductivity of air (W/m K);  $T_j$ : Jet temperature (°C);  $T_r$ : Temperature of the target plate in radial directions (°C).

#### 3. Results and discussion

## 3.1. Wall static pressure distribution

## 3.1.1. Independency test

The effect of *Re* (16,000 to 55,000) on static pressure (Cp) distribution was evaluated. During the test, z/d was maintained at 1.0, an optimal range to ensure a consistent jet impact regime. Cp was found to be independent of *Re* considered in this study (Fig. 4a). Despite the significant changes in flow dynamics, the Cp distribution at the impingement point does not show a substantial variation with *Re*. This can also be explained by the characteristics of the potential core region, where the jet velocity stays nearly constant as the turbulent mixing tends to stabilize the pressure distribution over the surface [13,26]. Further, the fundamental momentum transfer mechanism to the target surface remains largely unchanged. This leads to a consistent pressure distribution, as the high momentum flux ensures a stable impingement pressure [1,27].

The C<sub>p</sub> was found to be independent of *Re* considered in this study. Aforementioned, Re of values between 16,000 and 55,000 and it can be considered that the jet is predominantly in a turbulent regime. In this regime, the jet core develops a turbulent boundary layer that grows more rapidly, and the flow becomes more disordered and mixing intensifies. Despite these changes in flow dynamics, the C<sub>p</sub> distribution at the impingement point does not show significant variation with Re. This is because the turbulent mixing tends to stabilize the pressure distribution over the target plate, resulting in similar C<sub>p</sub> values despite varying Re. This can also be attributed to the characteristics of the potential core region, where the jet velocity remains almost constant. The pressure drop within this range is minimal because the jet retains its core velocity and energy. [13,26]. Further, the fundamental momentum transfer mechanism to the plate remains largely unchanged. This leads to a consistent pressure distribution, as the high momentum flux ensures a stable impingement pressure [1,27]. The controlled experimental conditions, including optimal jet-to-plate spacing, further support the conclusion that Cp remains unaffected by variations in Re, providing a

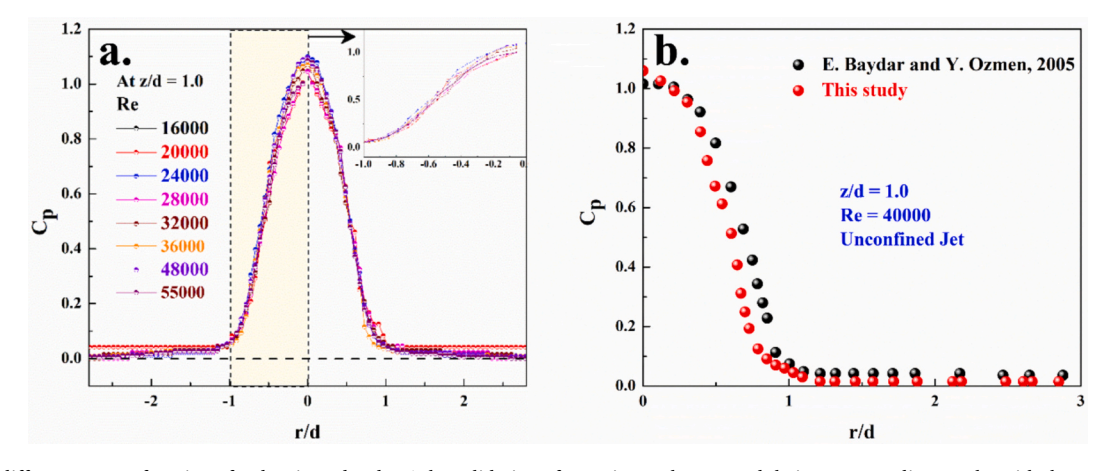


Fig. 4. a. Cp at different Re as a function of r/d ratio and z/d = 1; b. Validation of experimental setup and their corresponding results with the previously published results published elsewhere [28].

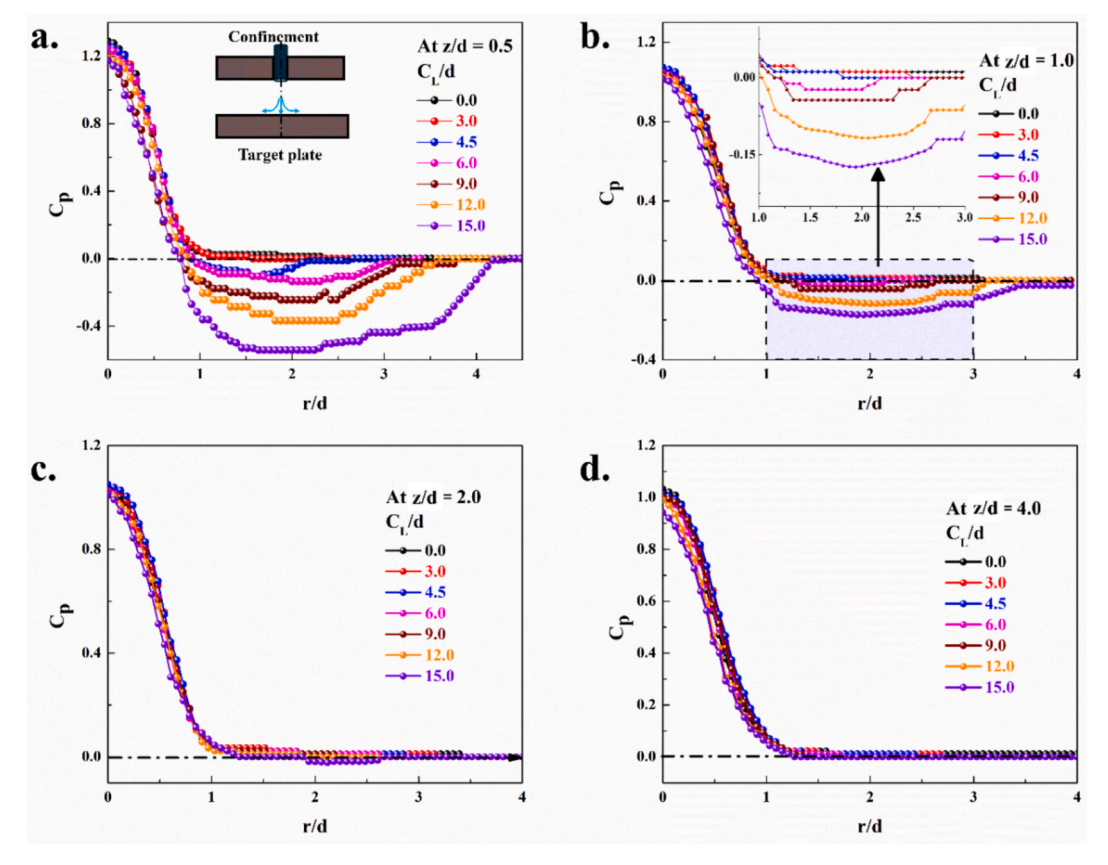


Fig. 5. Effect of degree of confinement on C<sub>p</sub> distribution at different z/d ratios and at a Re of 40,000; a. 0.5; b. 1.0; c. 2.0; d. 4.0.

robust understanding of the jet impingement dynamics.

A study was conducted with a baseline experiment to verify the accuracy of the experiments and subsequent pressure distribution results. To confirm and validate the harvested data, the Cp distribution for a jet impinging perpendicularly on a surface was correlated with the established data from the work of Baydar and Ozmen, published elsewhere [28]. Fig. 4b illustrates the Cp distribution evaluated at a Re of 40,000 and a z/d ratio of 1. The agreement between the two sets was within 3 %, indicating a high level of consistency and validating the experimental approach used in this study. This close correlation is consistent with previous results, further reinforcing the consistency and accuracy of the experimental setup and procedures.

#### 3.1.2. Effect of degree of confinement

The influence of various parameters, z/d ratio (0.0–6.0), r/d ratio (0.0–4.0), and confinement plate size ( $C_L/d$ : 0.0–15.0), on Cp distribution was evaluated. The Re was maintained at 40,000 for all the experiments, as this study is dedicated to examining the influence of confined turbulent jet. Fig. 5 a-d shows the Cp distribution with respect to r/d for different z/d and  $C_L/d$  values.

The static pressure was highest at the stagnation point for all  $C_L/d$  ratios considered in this study and decreased as the flow accelerated radially outwards from the stagnation point. No sub-atmospheric zone was observed for an unconfined impinging jet for any z/d values considered in this study (Fig. S2a). At z/d=0.5, a sub-atmospheric zone was extended for all the confined jets. The sub-atmospheric zone became stronger as the confinement size increased and was perceived to be susceptible to the z/d ratio and became weaker with the increase in z/d ratio. At  $C_L/d$ : 15.0, the sub-atmospheric zone was observed up to a z/d distance of 4.0, while it was observed only up to z/d: 2.0 for  $C_L/d$ : 12.0 and  $C_L/d$ : 6.0. However, for  $C_L/d$ : 3.0–4.5, there was no sub-atmospheric zone beyond z/d ratio of 0.5.

Fig. S2b shows the effect of z/d on the sub-atmospheric region for C<sub>I</sub>/

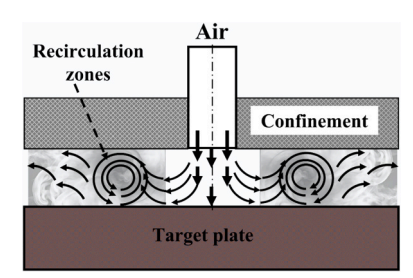


**Fig. 6.** Schematic illustration depicting the plausible recirculation zone formed due to the confinement effect.

d=15.0. This indicates that the sub-atmospheric pressure was sensitive to the confinement size. The presence of the sub-atmospheric zone could be attributed to an interplay of fluid behavior, pressure dynamics in a turbulent flow and jet interaction with the impinging plate surface. When a high-velocity jet strikes the flat impinging plate, it creates a region of high dynamic pressure. In a confined zone, the jet cannot dissipate freely, so it spreads radially along the surface of the impinging plate, which could further accelerate due to the constriction. As a result, the Cp further decreased, leading to the formation of a sub-atmospheric zone. This dynamic leads to the formation of recirculation zones, where the flow moves in the opposite direction to the original jet path, creating swirling or vortex-like structures in the wake (Fig. 6).

These recirculation zones are characterized by reverse flow patterns and increased mixing, driven by pressure recovery and the development of boundary layers near the surface. The confined space also forces the jet to adapt, causing flow separation and turbulent wake regions that further contribute to recirculation. Furthermore, the sub-atmospheric zone shifted linearly radially outward from the stagnation point with the increase in the z/d ratio (Fig. 7a). This phenomenon could be

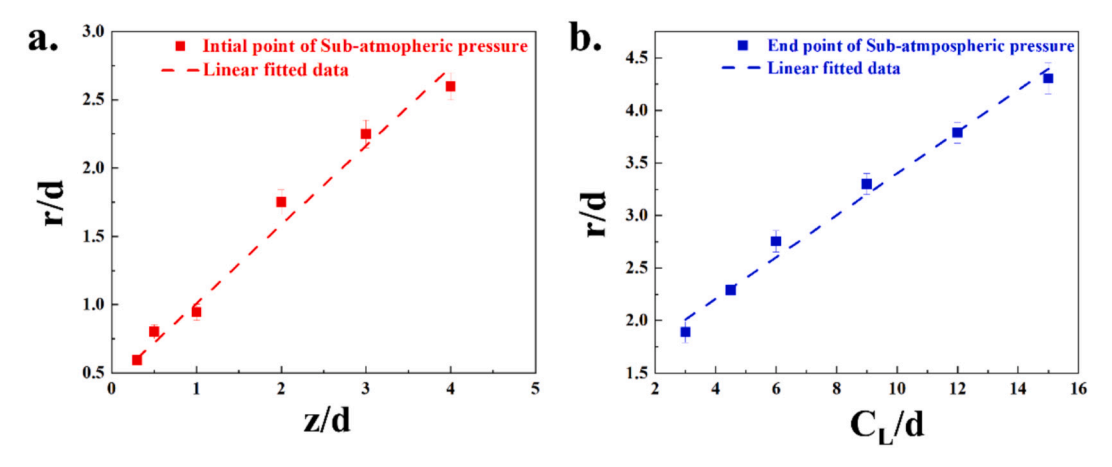


Fig. 7. a. Initiation of sub-atmospheric pressure zone in relation to z/d ratio for  $C_L/d = 15.0$ ; b. End of sub-atmospheric zone with respect to r/d ratio and degree of confinement at a z/d ratio of 0.5.

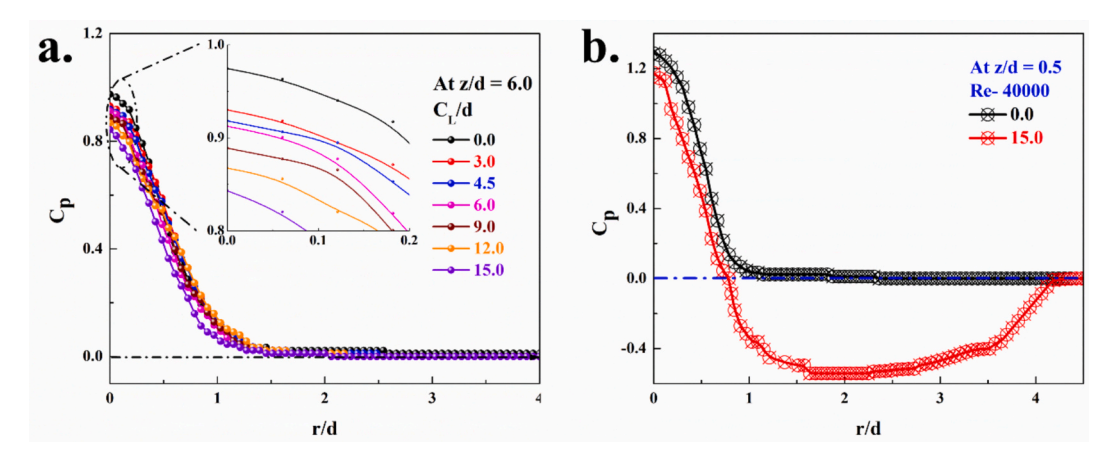
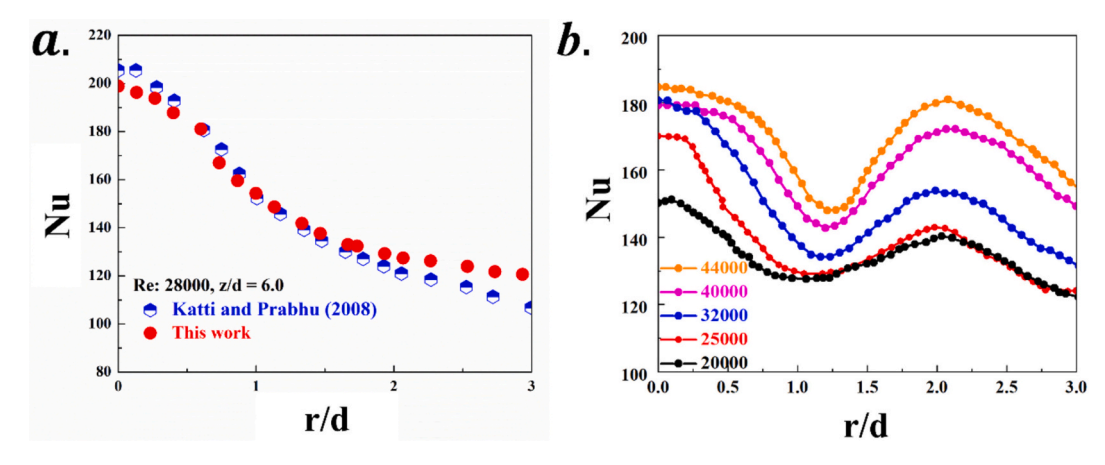


Fig. 8. a. Effect of degree of confinement on  $C_p$  distribution at z/d ratio of 6.0; b. Comparison of confined ( $C_L/d = 15.0$ ) and unconfined jet ( $C_L/d = 0.0$ ) on  $C_p$  distribution depicting the formation of sub-atmospheric zone.

ascribed to the reduction in the jet velocity as it spreads with increasing z/d ratio and subsequently, the sub-atmospheric zone also became weaker [28,29]. On the other hand, a clear linear trend in the recovery of sub-atmospheric pressure as a function of  $C_L/d$  and r/d ratio. This trend indicated that the sub-atmospheric zones were broader with the increase in the  $C_L/d$  ratio (Fig. 7b).

Also, as z/d ratio increased, the velocity of the jet declined due to the

jet spreading, and thus, the intensity of the sub-atmospheric zone decreased. Subsequently, the stagnation pressure decreased. On the other hand, in an unconfined jet, a sub-atmospheric zone was not observed because the jet can expand freely into the surrounding environment without the constraints that cause significant pressure drops. When a high-velocity jet exits a nozzle in an unconfined space, it entrains and mixes with the ambient fluid, allowing the pressure to



**Fig. 9.** a. Validation of experimental setup and its corresponding Nu values with the previously published results published elsewhere [23]; b. Nu as a function of Re for a confined impinging jet  $(C_L/d = 12.0; z/d = 1.0)$ .

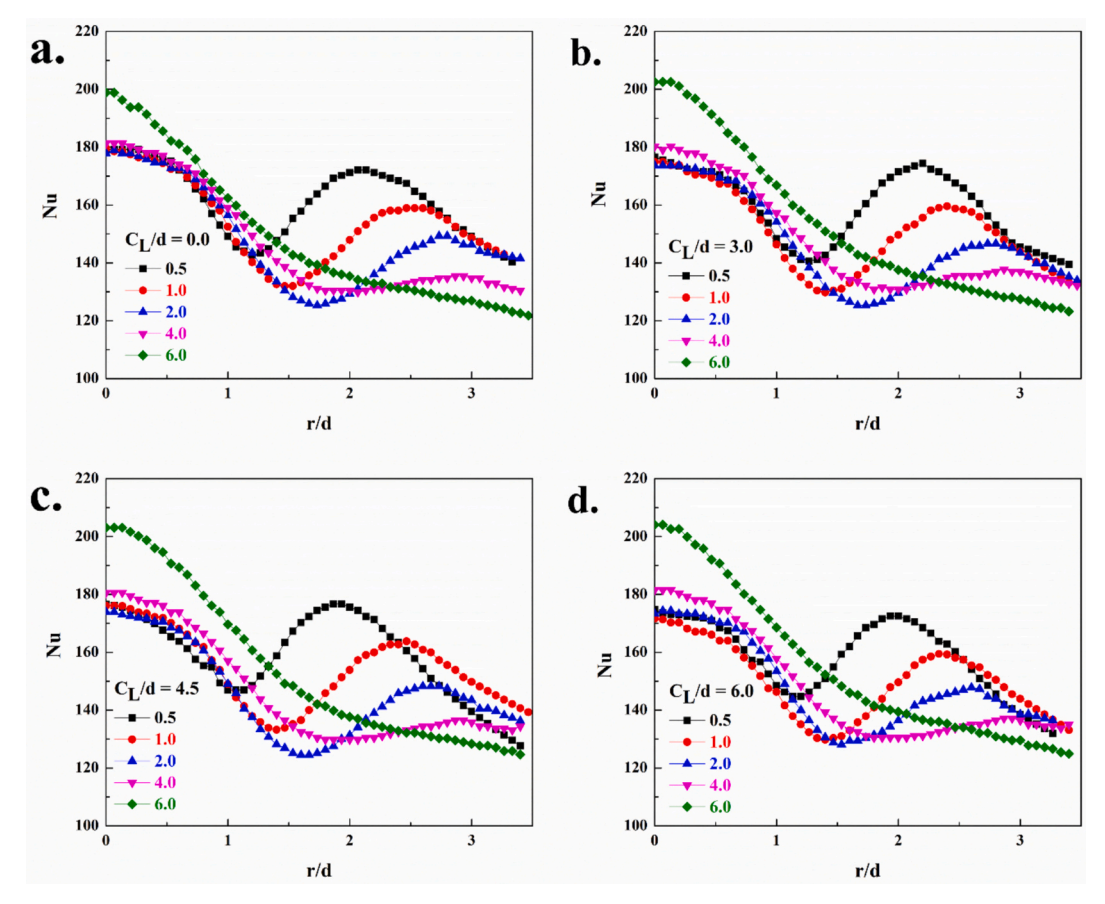


Fig. 10. Effect of degree of confinement ( $C_L/d$ ) on Nu at different z/d ratios and at a Re of 40,000; a.  $C_L/d$ : 0.0; b.  $C_L/d$ : 3.0; c.  $C_L/d$ : 4.5; d.  $C_L/d$ : 6.0.

equalize more rapidly than in a confined scenario. This free expansion mitigates the creation of low-pressure regions since the fluid can spread out and decelerate gradually without encountering restrictive boundaries that would otherwise amplify the pressure drop. Additionally, the ambient fluid's unrestricted interaction with the jet promotes efficient mixing and diffusion, further preventing the formation of localized subatmospheric zones [8,27,30]. At z/d=6.0, no negative pressure was observed for either confined or unconfined cases (Fig. 8a). In fact, the pressure distribution in both scenarios exhibited similar trends, indicating that confinement effects were negligible beyond z/d=4.0. At z/d=6.0, the air had sufficient space to exit without restrictions, behaving similarly to an unconfined jet. Fig. 8b illustrates the significance of the degree of confinement compared to the unconfined air jet, depicting the formation of negative Cp in confined air jet.

# 3.2. Heat transfer characteristics

A horizontal axis impinging jet flow setup was built to investigate the heat transfer characteristics on a flat, smooth plate in an impinging confined jet flow field. The Re was maintained at 40,000 across various z/d ratios as a function of r/d and degree of confinement. Experiments were conducted with an unconfined jet at a z/d value of 6.0, to validate the results and compare the obtained results with previous studies published elsewhere [23]. The present study showed a strong correlation and the Nu values are in line with the previous published data (Fig. 9a). A typical curve of Nu as a function of Re for  $C_L/d$  of 12.0 at z/d ratio of 1.0 (Fig. 9b). At a particular z/d and r/d ratio, the Nu values increased with the increase in Re, which is also well reported in the literature. As the Re increased, the fluid flow becomes chaotic leading to a more swirling, fluctuating, and rapidly changing velocities, which significantly enhances mixing and resulted in increased heat transfer. At

the stagnation point, the high-velocity jet impinged on the target plate, creating a primary peak in the heat transfer distribution. Additionally, a secondary peak was also observed beyond an r/d of 1.0, which intensified with increasing Re. This phenomenon can be attributed to the radial spreading of the jet, where the airflow intensifies the shear layer with increasing Re [10,31,32].

Fig. 10a-d and Fig. 11 a-d shows the Nu distributions obtained from the temperature values harvested along the target plate on the smooth flat plate at different C<sub>I</sub>/d and z/d ratios. For all the configurations, the Nu was maximum at the stagnation point and decreased along the radial direction up to r/d  $\approx$  1.0; thereafter, an abrupt increase in the *Nu* was observed and subsequently, a secondary peak was observed. At stagnation point, for all the z/d spacing (<4.0) the Nu was higher for the unconfined jet and decreased with the increase in confinement size (C<sub>L</sub>/ d = 3.0-15.0) (Fig. 12a). Furthermore, with increasing z/d spacing, the secondary Nu value peak shifted radially outward in both unconfined and confined jet configurations due to changes in flow dynamics and turbulence characteristics. For a lower z/d ratio, the jet impacts the target surface directly at the stagnation point with negligible interaction with ambient air, causing the secondary peak to form close to the stagnation point. However, as the z/d ratio increased, the jet had more room to develop turbulence and spread radially before impinging on the plate led to a further shift of the secondary peak. This phenomenon also indicate that the recirculation zones shifted outwards with increasing z/ d ratio [33,34].

Interestingly, at a particular z/d ratio and with increasing confinement size, the secondary peak tends to form closer to the stagnation point (Fig. 12b). In confined jets, the side walls slightly restrict the radial spread, but the overall trend of the secondary peak shifting with increased spacing continued. This behavior is critical for optimizing heat transfer systems, as it allows designers to manipulate z/d spacing to

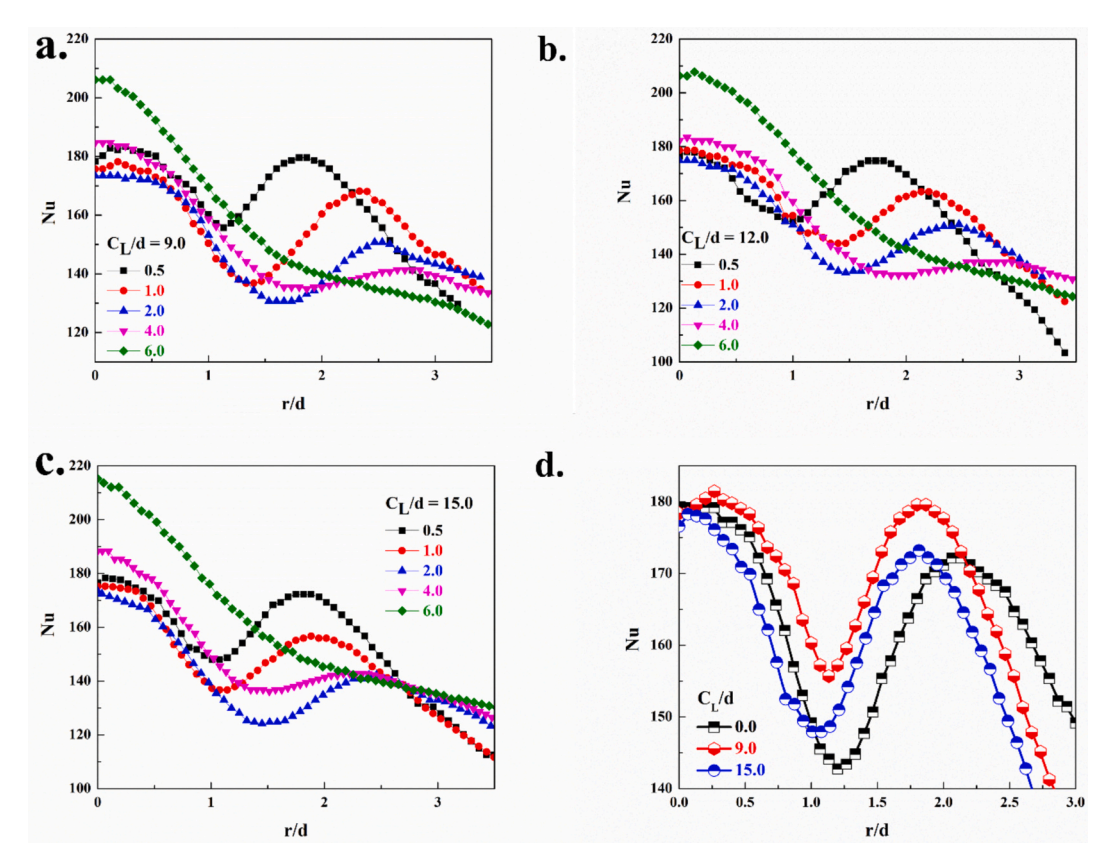


Fig. 11. Effect of degree of confinement ( $C_L/d$ ) on Nu at different z/d ratios and at a Re of 40,000; a.  $C_L/d$ : 9.0; b.  $C_L/d$ :12.0; c.  $C_L/d$ : 15.0; d. Unconfined and confinement effect on Nu specifically depicting the variation in the intensity of secondary maxima at z/d = 0.5.

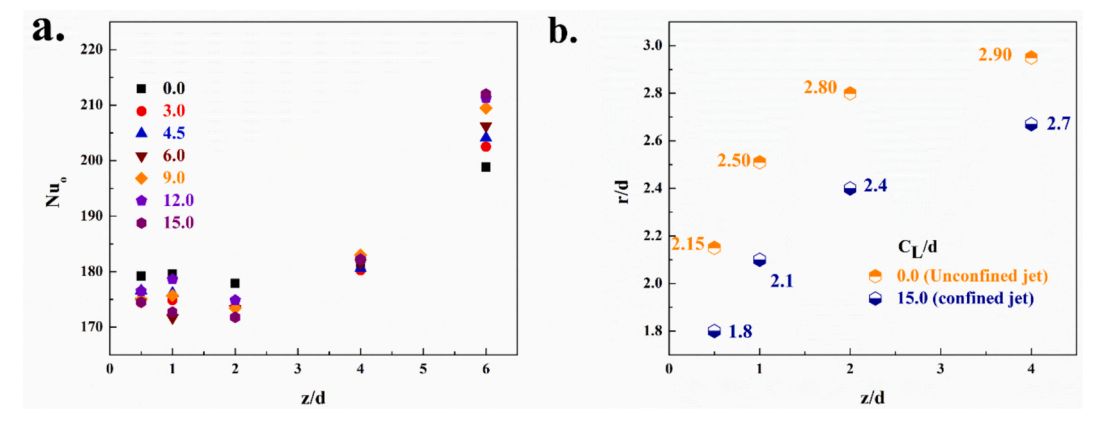


Fig. 12. a. Nu at stagnation at different z/d ratio and degree of confinement; b. Lateral shift in the secondary peak values as a function of degree of confinement.

achieve efficient and uniform heat transfer across the impinging surface. Understanding these dynamics is essential for applications such as cooling electronic components or turbine blades, where precise control over the heat transfer distribution is crucial.

Furthermore, at z/d=6.0, the  $\mathit{Nu}$  values increased dramatically, compared to lower z/d ratios. The  $\mathit{Nu}$  was seen to be higher at the stagnation point and decreased along the radial direction. Moreover, with the increase in the confinement size, the  $\mathit{Nu}$  values increased at the stagnation point. For instance, at  $C_L/d=0.0$ , the  $\mathit{Nu}$  value at the stagnation point was 198.1, which increased to 215 for  $C_L/d=15.0$  (Fig. S3a). The increase in the  $\mathit{Nu}$  at z/d spacing of 6.0 increased with the increase in confinement sizes, contrary to the trend observed at a lower plate spacing, which could be attributed to the change in flow dynamics and turbulent characteristics. At higher plate spacings, the jet required

to cover a larger distance to develop turbulence before impinging on the plate. This leads to enhanced mixing and disruption of the thermal boundary layer and increases heat transfer rates around the stagnation region. A similar trend was observed in previous research carried out elsewhere [29,35,36]. With the increase in confinement size, the flow of the jet is restricted, which could have promoted the turbulence formation and better mixing.

Furthermore, at higher z/d spacings, such as z/d=6.0, the absence of a secondary peak across all configurations can be explained by the jet's behavior after impinging on the target plate. When the jet strikes the plate from a greater distance, it spreads more easily, losing intensity and coherence. This results in a decreased intensity and allows the jet to transition gradually along the impinging wall, leading to a weaker heat transfer distribution without localized intensification. Consequently, the

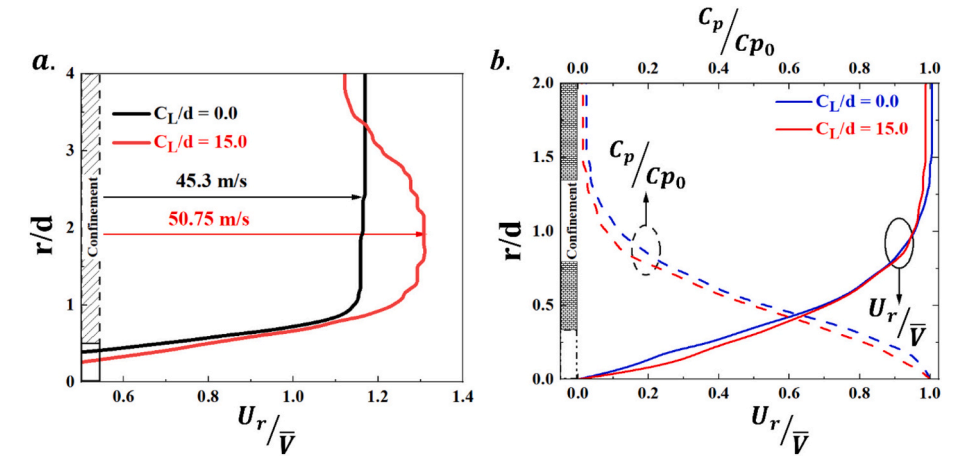


Fig. 13. Velocity profiles of unconfined and confined jets in the radial direction; a. z/d=0.5; b. z/d=6.0 ( $\overline{V}=$  Average velocity of air at jet exit;  $U_r=$  Relative velocity of air after impingement).

secondary peak diminishes at these higher plate spacings. This trend is consistently observed across all configurations, with the secondary peak becoming weaker as the z/d spacing increases (z/d < 4.0).

To summarize, the influence of confinement size was particularly noticeable in the region where the secondary peak typically occurred. It was found that the secondary peak increased with the increase in confinement size (up to  $C_I/d = 12.0$ ) in a turbulent jet, but it weakened slightly upon further increasing the confinement size, which indicates that the confined spaces readily promote flow recirculation leading to enhanced heat transfer performance. However, this effect weakened when the confinement size approached the size of the target plate (C<sub>L</sub>/d = 15.0). On the other hand, at higher C<sub>L</sub>/d ratios, the formation of the recirculation zone occurs close to the stagnation point as confirmed in the fluid flow studies. This could have disrupted the development of the wall jet and contributed to the formation of more complex and chaotic flow regimes. The recirculation zones interfere with the incoming jet, affecting the radial spreading, which may have resulted in velocity fluctuations and lead to disrupting the thermal and velocity boundary layers. Therefore, the overall effect on heat transfer coefficients increased. Overall, it is vital to maintain the confinement size smaller than the target surface is essential for achieving optimal heat transfer performance.

In several previous studies typically considered confinement sizes equal to or greater than the target plate size and no significant difference in heat transfer compared to unconfined jets. In fact, several studies reported a decline in Nu values with the use of confinement for jet impingement [9,17,20,37,38]. Moreover, the effect of radial jet spreading after impingement on the target surface and its impact on fluid flow and heat transfer characteristics have not been thoroughly addressed. The current findings highlight the significant role that confinement size plays in modulating heat transfer coefficients in impinging jets. On the other hand, the comparison of this work with the previous work on confined jet carried out by Baydar and Ozmen [39] (Fig. S3b), indicating significant enhancement in heat transfer performance. Moreover, the increase in the secondary maxima with larger confinement sizes can be ascribed to the formidable interaction between the jet flow and the confinement walls. As the confinement wall size increased, the radial jet flow intensified the turbulence within the confined space. This heightened turbulence enhances heat transfer by promoting better mixing and boundary layer disruption, increasing secondary peak value [40,41]. Additionally, in confined jets, particularly at larger C<sub>I</sub>/d ratio, forming sub-atmospheric pressure regions can enhance the entrainment of surrounding fluid locally, confirming the strong linkage between fluid flow and heat transfer characteristics [38].

Fig. 13a illustrates the near-wall velocity profiles of unconfined and

confined jet in the radial direction for a z/d spacing of 0.5. When the impinging jet strikes the target surface, the static pressure reaches a maximum, while the velocity abruptly drops to zero due to the sudden loss of momentum. Subsequently, the fluid changes direction and accelerates radially outward along the target surface. As a result, the radial velocity increased with radial distance from the stagnation point, while the corresponding Cp exhibits an inverse trend. In this study, the nearwall velocity profiles for  $C_I/d = 0.0$  and  $C_I/d = 15.0$  were specifically compared, as the profiles for other confinement sizes fell between these two limiting cases. In both unconfined and confined jets, the maximum velocity occurred within the r/d range of 1.0-2.5. Notably, upon confinement, the near-wall velocity values increased compared to those of the unconfined jet, which can be attributed to the vertical flow restriction due to the confinement wall. In the case of an unconfined jet, the air exits progressively in the radial direction, whereas confinement introduces an abrupt transition, which may have given rise to a whirling effect. This behavior leads to a pronounced peak in the velocity profile, contributing to an enhanced secondary local heat transfer peak. Furthermore, the increased velocity values observed in the confined jet resulted in higher secondary local heat transfer peak values. Another observation is that in the confined jet, the near-wall velocity decays rapidly as the air expands radially outward. This behavior directly correlates with local heat transfer distributions, where the increased secondary heat transfer peak values in the confined case diminish swiftly with radial distance. At a higher z/d spacing of 6.0, no substantial difference was observed in the velocity profile trends between unconfined and confined jets (Fig. 13b). In both cases, the maximum near-wall velocity was located away from the stagnation point, without any abrupt variations in the velocity profiles. This indicates that, at larger z/ d spacings, the influence of confinement becomes negligible allowing the air to expand freely in the radial direction. The results exhibit good consistency with the pressure studies. As z/d increased, the radial location of the maximum velocity shifted further from the stagnation region, leading to a corresponding shift in the position of the secondary local heat transfer peak. These findings confirm that the near-wall velocity profiles are closely correlated with the underlying fluid flow structures and associated heat transfer characteristics.

Further, the thermal performance factor (TPF) was determined using the following equations

$$TPF = \frac{Nu/Nu_o}{f/f_o}$$
 (6)

and

**Table 1** TPF as a function of confinement ratio  $(C_I/d)$ .

Confinement ratio (C <sub>L</sub> /d)	TPF at $z/d = 0.5$	TPF at $z/d = 6.0$
0	_	_
3.0	0.98	1.06
4.5	1.03	1.09
6.0	1.07	1.09
9.0	1.40	1.11
12.0	1.42	1.15
15.0	1.38	1.18

$$f = \frac{2 \times \Delta P}{\rho \times \overline{V}^2} \tag{7}$$

Where,  $\Delta P=$  change in static pressure;  $\rho=$  Density;  $\overline{V}=$  Average velocity at jet exit;  $U_r=$  Relative velocity after impingement;  $Nu_0=Nu$  values of unconfined jet considered as reference; f and  $f_o$  are the friction factor with and without confinement, respectively.

The TPF increased with increasing confinement ratio (Table 1). The increase in the TPF with confinement ratio indicates that confining the nozzle wall is beneficial in defining the flow dynamics and thermal behavior in the impingement jets. As confirmed in the fluid flow and heat transfer results, the sub-atmospheric pressure could have led to an increase in turbulence intensity and promoted local heat transfer coefficients. The heat transfer rate overcomes the necessary friction loss upon confinement of the nozzle, leading to net gain in TPF.

Fig. 14a and b illustrates the temperature distribution on a flat surface subjected to an unconfined and confined impinging jet impacted from an interplate spacing of 0.5. In the case of unconfined jet, the jet entrains ambient fluid freely and the temperature distribution remained symmetric and concentrated near the stagnation point (Fig. 14a). In contrast, confined jet the nonconformities in the flow structure was

observed (Fig. 14b). The presence of confinement walls hindered the ambient entrainment air leading to the lateral spreading of the jet, which resulted in increased radial temperature gradients. As a result, it is possible that the heat transfer effect at the stagnation point may have slightly diminished, while radial heat transfer is elevated due to a broader temperature distribution. This suggests that the confinement promotes more effective radial heat transfer effects. On the other hand, for higher inter-plate spacings (z/d=6.0), the jet dissipation became more pronounced in the case of an unconfined jet, which is a well-established study. For  $C_L/d=0.0$ , the jet showed a smoother yet center-focused cooling profile, while the effect was seen to be significantly pronounced not only at the stagnation point, but also propagated radially (Fig. 14c and d).

From an application perspective, the outcomes of this work have significant implications for various industries. In the cooling of electronic components, the insights into how confinement size and nozzleto-plate spacing affect heat transfer can lead to more efficient cooling solutions, essential for preventing overheating and ensuring the longevity of electronic devices. Similarly, in gas turbines, optimized impinging jet systems can enhance the cooling efficiency of turbine blades, thereby improving operational efficiency and extending the lifespan of the blades. In material processing, such as drying, heating, or surface treatment, the improved understanding of heat transfer dynamics can lead to more uniform and controlled thermal processes, enhancing product quality and process consistency. Furthermore, in future insights, exploring different jet configurations, such as multiple jets, inclined jets, or oscillating jets, could provide a deeper understanding of their impact on heat transfer characteristics. Also, investigating the effects of different target plate materials and surface textures could also yield valuable insights, as these factors can significantly influence the heat transfer efficiency.

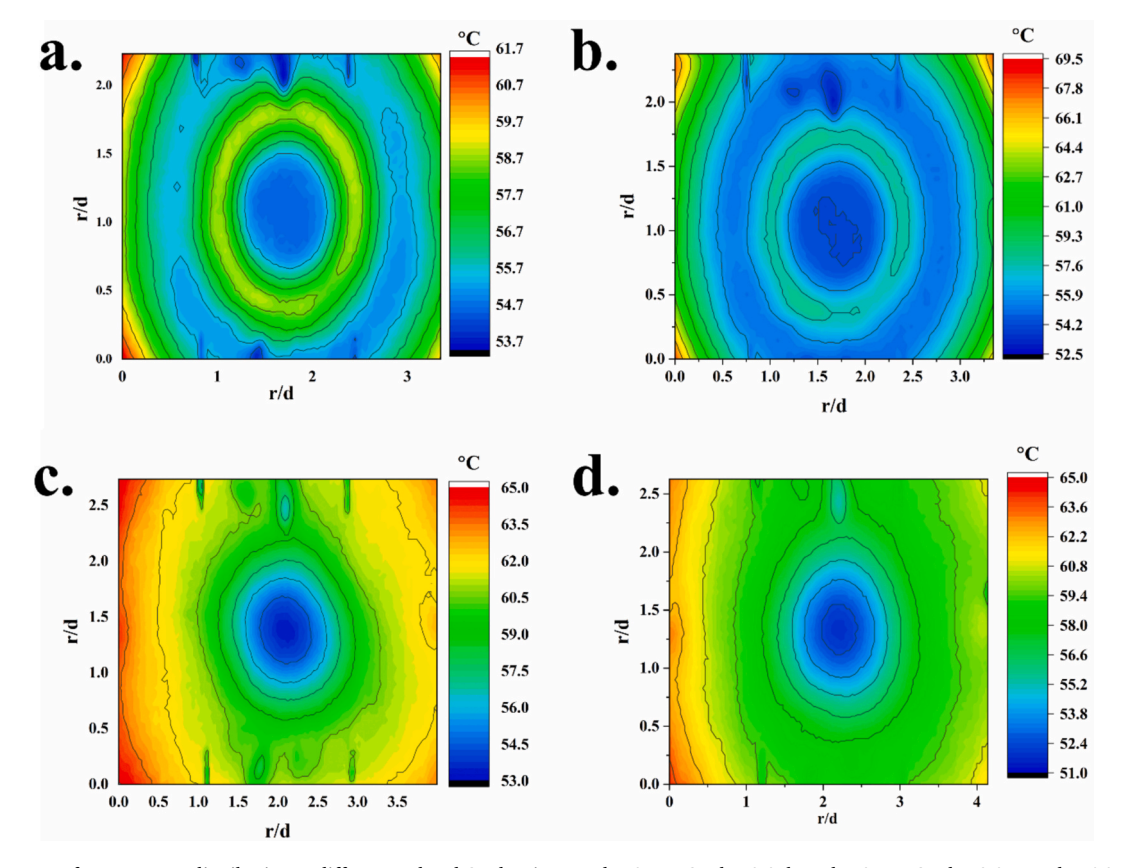


Fig. 14. Contour map of temperature distribution at different z/d and  $C_L/d$  ratio; a. z/d=0.5 at  $C_L/d=0.0$ ; b. z/d=0.5 at  $C_L/d=9.0$ ; c. z/d=6.0 at  $C_L/d=0.0$ ; d. z/d=6.0 at  $C_L/d=15.0$ .

#### 4. Conclusions

An experimental study examined the impact of confinement size on static pressure distribution and Nusselt number (Nu) of a turbulent air jet impinging on a flat target plate. Various confinement sizes (C<sub>L</sub>/d = 0.0 to 15.0) and z/d ratios (0.5 to 6.0) were examined. Wall static pressure was highest at stagnation and decreased laterally, with increased sub-atmospheric pressure and recirculation zones observed with larger confinements. Heat transfer at stagnation decreased with larger confinements, while C<sub>L</sub>/d and z/d spacing influenced a secondary peak in Nu. The secondary peak intensified with confinement up to C<sub>L</sub>/d = 12.0 and weakened upon further increase in the confinement size, which is attributed to the change in the flow regime. At z/d = 6.0, heat transfer at stagnation increased with confinement size. Also, maintaining the confinement size smaller than the target surface is essential for achieving optimal heat transfer performance. This study provides critical insights for optimizing impinging jet systems, revealing the nuanced interplay between fluid dynamics and heat transfer coefficients. Therefore, it is concluded that achieving high heat transfer coefficients for efficient cooling requires optimizing inter-plate spacing, Re and confinement size. This insight is crucial for researchers and industries, providing essential guidance for designing more effective impinging air jet systems.

## CRediT authorship contribution statement

Vijaykumar Nagathan: Writing – review & editing, Writing – original draft, Resources, Project administration, Data curation. Mohammed Khalifa: Writing – review & editing, Writing – original draft, Validation, Methodology, Investigation, Data curation. Basavaraj M. Angadi: Writing – review & editing, Validation, Supervision, Software, Resources. Meda Adimurthy: Writing – review & editing, Validation, Software, Formal analysis, Data curation. Vadiraj Katti: Writing – review & editing, Visualization, Validation, Supervision, Funding acquisition, Conceptualization.

#### **Funding details**

This work is part of the "Local heat transfer and Fluid Flow distributions due to Impinging synthetic Jets" project, which is funded by the Visvesvaraya Technological University (VTU) Research grant.

# Declaration of competing interest

The authors declare that they have no known competing financial interests or personal relationships that could have appeared to influence the work reported in this paper. We also declare that the authors did not use any generative AI tools in this study.

#### Acknowledgments

"This work is dedicated to Prof. Vadiraj Katti, whose invaluable guidance, support in securing funding, and pivotal role in translating the idea into practice were instrumental to the success of this project".

The authors would like to thank B.L.D.E. A's V.P. Dr. P. G. Halakatti College of Engineering and Technology, Vijayapur, Karnataka, India, for providing research facilities. M. Khalifa would like to thank Prof. S Anandhan (Department of Metallurgical and Materials Engineering, National Institute of Technology Karnataka) and DI. Herfried Lammer, Dr. Arunjunai Raj Mahendran (Kompetenzzentrum Holz GmbH, Austria) for their continuous support.

# Appendix A. Supplementary data

Supplementary data to this article can be found online at https://doi.org/10.1016/j.icheatmasstransfer.2025.109683.

#### Data availability

Data will be made available on request.

#### References

- R.D. Plant, J. Friedman, M.Z. Saghir, A review of jet impingement cooling, Int. J. Thermofluids 17 (2023) 100312, https://doi.org/10.1016/j.ijft.2023.100312.
- [2] G. Nasif, A.M. Shinneeb, R. Balachandar, Cooling enhancement for engine parts using jet impingement, Front, Mech. Eng. 10 (2024) 1–13, https://doi.org/ 10.3389/fmech.2024.1251587.
- [3] O.J. Wai, P. Gunnasegaran, H. Hasini, A review on experimental and numerical investigations of jet impingement cooling performance with Nanofluids, Micromachines 13 (2022), https://doi.org/10.3390/mi13122059.
- [4] M. Nirmalkumar, V. Katti, S.V. Prabhu, Local heat transfer distribution on a smooth flat plate impinged by a slot jet, Int. J. Heat Mass Transf. 54 (2011) 727–738, https://doi.org/10.1016/j.ijheatmasstransfer.2010.09.030.
- [5] P. Hrycak, D.T. Lee, J.W. Gauntner, J.N.B. Livingood, Experimental Flow Characteristics of a Single Turbulent Jet Impinging on a Flat Plate. https://ntrs. nasa.gov/citations/19700011262, 1970.
- [6] S.D. Barewar, M. Joshi, P.O. Sharma, P.S. Kalos, B. Bakthavatchalam, S. S. Chougule, K. Habib, S.K. Saha, Optimization of jet impingement heat transfer: a review on advanced techniques and parameters, Therm. Sci. Eng. Prog. 39 (2023), https://doi.org/10.1016/j.tsep.2023.101697.
- [7] Y.J. Choo, B.S. Kang, Parametric study on impinging-jet liquid sheet thickness distribution using an interferometric method, Exp. Fluids 31 (2001) 56–62, https://doi.org/10.1007/s003480000258.
- [8] S.V. Garimella, R.A. Rice, Confined and submerged liquid jet impingement, J. Heat Transfer 1 (2016). http://heattransfer.asmedigitalcollection.asme.org/ (on 01/28/2016).
- [9] K.S. Choo, S.J. Kim, Comparison of thermal characteristics of confined and unconfined impinging jets, Int. J. Heat Mass Transf. 53 (2010) 3366–3371, https:// doi.org/10.1016/j.ijheatmasstransfer.2010.02.023.
- [10] D. Lytle, B.W. Webb, Air jet impingement heat transfer at low nozzle-plate spacings, Int. J. Heat Mass Transf. 37 (1994) 1687–1697, https://doi.org/10.1016/ 0017-9310(94)90059-0.
- [11] V.V. Katti, S.N. Yasaswy, S.V. Prabhu, Local heat transfer distribution between smooth flat surface and impinging air jet from a circular nozzle at low Reynolds numbers, Heat Mass Transf. Und Stoffuebertragung 47 (2011) 237–244, https:// doi.org/10.1007/s00231-010-0716-1.
- [12] M. Adimurthy, V.V. Katti, Local distribution of wall static pressure and heat transfer on a smooth flat plate impinged by a slot air jet, Heat Mass Transf. Und Stoffuebertragung 53 (2017) 611–623, https://doi.org/10.1007/s00231-016-1847.0
- [13] H. Fellouah, C.G. Ball, A. Pollard, Reynolds number effects within the development region of a turbulent round free jet, Int. J. Heat Mass Transf. 52 (2009) 3943–3954, https://doi.org/10.1016/j.jiheatmasstransfer.2009.03.029.
- [14] J.B.R. Loureiro, A.P. Silva Freire, Velocity and temperature profiles, wall shear stress and heat transfer coefficient of turbulent impinging jets, Int. J. Heat Mass Transf. 107 (2017) 846–861, https://doi.org/10.1016/j. iiheatmasstransfer.2016.10.105.
- [15] N.T. Obot, W.J.M. Douglas, A.A. Mujumdar, Effect of semi-confinement on impingement heat transfer, Heat Transf. Proc. Int. Heat Transf. Conf. (1982) 389–394, https://doi.org/10.1615/ihtc7.2030.
- [16] W. Zhao, K. Kumar, A.S. Mujumdar, Flow and heat transfer characteristics of confined noncircular turbulent impinging jets, Drying Technol. 22 (2004) 2027–2049, https://doi.org/10.1081/DRT-200034239.
- [17] J.Y. San, C.H. Huang, M.H. Shu, Impingement cooling of a confined circular air jet, Int. J. Heat Mass Transf. 40 (1997) 1355–1364, https://doi.org/10.1016/S0017-9310(96)00201-3.
- [18] E. Baydar, Confined impinging air jet at low Reynolds numbers, Exp. Therm. Fluid Sci. 19 (1999) 27–33, https://doi.org/10.1016/S0894-1777(98)10044-4.
- [19] J.A. Fitzgerald, S.V. Garimella, Visualization of the flow field in a confined and submerged impinging jet, Am. Soc. Mech. Eng. Heat Transf. Div. HTD 346 (1997)
- [20] Y.J. Youn, K. Choo, S.J. Kim, Effect of confinement on heat transfer characteristics of a microscale impinging jet, Int. J. Heat Mass Transf. 54 (2011) 366–373, https://doi.org/10.1016/j.ijheatmasstransfer.2010.09.035.
- [21] T. Guo, M.J. Rau, P.P. Vlachos, S.V. Garimella, Axisymmetric wall jet development in confined jet impingement axisymmetric wall jet development in confined jet impingement, Phys. Fluids 29 (2017) 025102-1-1-1-12, https://doi.org/10.1063/ 14075304
- [22] J.Y. San, W.Z. Shiao, Effects of jet plate size and plate spacing on the stagnation Nusselt number for a confined circular air jet impinging on a flat surface, Int. J. Heat Mass Transf. 49 (2006) 3477–3486, https://doi.org/10.1016/j. ijheatmasstransfer.2006.02.055.
- [23] V. Katti, S.V. Prabhu, Experimental study and theoretical analysis of local heat transfer distribution between smooth flat surface and impinging air jet from a circular straight pipe nozzle, Int. J. Heat Mass Transf. 51 (2008) 4480–4495, https://doi.org/10.1016/j.ijheatmasstransfer.2007.12.024.
- [24] V. Nagathan, M. Khalifa, A. Hussain, B. Basavaraj, M.A. Vadiraj, Dynamics of subatmospheric zones and their impact on the fluid flow and heat transfer characteristics of impinging air jet on circular standalone ribbed targets, Heat Mass

- Transf. Und Stoffuebertragung 61 (2025) 1–14, https://doi.org/10.1007/s00231-025-03572-6
- [25] R.J. Moffat, Describing the uncertainties in experimental results, Exp. Thermal Fluid Sci. 1 (1988) 3–17, https://doi.org/10.1016/0894-1777(88)90043-X.
- [26] J.N.B. Livingood, P. Hrycak, Impingement Heat Transfer from Turbulent Air Jets to Flat Plates: A Literature Survey. http://hdl.handle.net/2060/19730016200, 1973.
- [27] K. Jambunathan, E. Lai, M.A. Moss, B.L. Button, A review of heat transfer data for single circular jet impingement, Int. J. Heat Fluid Flow 13 (1992) 106–115, https://doi.org/10.1016/0142-727X(92)90017-4.
- [28] E. Baydar, Y. Ozmen, An experimental and numerical investigation on a confined impinging air jet at high Reynolds numbers, Appl. Therm. Eng. 25 (2005) 409–421, https://doi.org/10.1016/j.applthermaleng.2004.05.016.
- [29] S.S. Hsich, J.T. Huang, H.H. Tsai, Heat transfer of confined circular jet impingement, J. Mech. 17 (2001) 29–38, https://doi.org/10.1017/ s1727719100002392
- [30] D.W. Colucci, R. Viskanta, Effect of nozzle geometry on local convective heat transfer to a confined impinging air jet, Exp. Therm. Fluid Sci. 13 (1996) 71–80, https://doi.org/10.1016/0894-1777(96)00015-5.
- [31] J.C. Akfirat, F.M. Company, The role of turbulence in determining the heat-transfer characteristics of impinging jets, Int. J. Heat Mass Transf. 8 (1965) 1261–1272. http://www.sciencedirect.com/science/article/pii/0017931065900542.
- [32] M. Daadoua, B. Mathew, F. Alnaimat, Experimental investigation of pressure drop and heat transfer in minichannel with smooth and pin fin surfaces, Int. J. Thermofluids 21 (2024) 100542, https://doi.org/10.1016/j.ijft.2023.100542.
- [33] S.V. Garimella, V.P. Schroeder, Local heat transfer distributions in confined multiple air jet impingement, J. Electron. Packag. Trans. ASME 123 (2001) 165–172, https://doi.org/10.1115/1.1371923.

- [34] S. Yao, Y. Guo, N. Jiang, J. Liu, An experimental study of a turbulent jet impinging on a flat surface, Int. J. Heat Mass Transf. 83 (2015) 820–832, https://doi.org/ 10.1016/j.ijheatmasstransfer.2014.12.026.
- [35] P. Gulati, V. Katti, S.V. Prabhu, Influence of the shape of the nozzle on local heat transfer distribution between smooth flat surface and impinging air jet, Int J Therm Sci 48 (2009) 602–617, https://doi.org/10.1016/j.ijthermalsci.2008.05.002.
- [36] H. Keles, Y. Özmen, Experimental investigation of heat transfer effects in impinging circular jets confined by inclined plates, Int. J. Heat Fluid Flow 108 (2024), https://doi.org/10.1016/j.ijheatfluidflow.2024.109468.
- [37] A.M. Huber, R. Viskanta, Effect of jet-jet spacing on convective heat transfer to confined, impinging arrays of axisymmetric air jets, Int. J. Heat Mass Transf. 37 (1994) 2859–2869, https://doi.org/10.1016/0017-9310(94)90340-9.
- [38] T. Guo, M.J. Rau, P.P. Vlachos, S.V. Garimella, Axisymmetric wall jet development in confined jet impingement, Phys. Fluids 29 (2017), https://doi.org/10.1063/ 1.4975394.
- [39] E. Baydar, Y. Ozmen, An experimental investigation on flow structures of confined and unconfined impinging air jets, Heat Mass Transf. Und Stoffuebertragung 42 (2006) 338–346, https://doi.org/10.1007/s00231-005-0021-6.
- [40] F.V. Barbosa, S.F.C.F. Teixeira, J.C.F. Teixeira, Convection from multiple air jet impingement - a review, Appl. Therm. Eng. 218 (2023), https://doi.org/10.1016/j. applthermaleng.2022.119307.
- [41] F. Schwertfirm, J. Gradl, H.C. Schwarzer, W. Peukert, M. Manhart, The low Reynolds number turbulent flow and mixing in a confined impinging jet reactor, Int. J. Heat Fluid Flow 28 (2007) 1429–1442, https://doi.org/10.1016/j. ijheatfluidflow.2007.04.019.